J. Astrophys. Astr. (1987) **8,** 17–31

N-Body Simulations of Tidal Encounters between Stellar Systems

P. Devadas Rao* & N. Ramamani *Centre of Advanced Study in Astronomy, Osmania University, Hyderabad 500007*

Saleh Mohammed Alladin† *International Centre for Theoretical Physics,* 34100 *Trieste, Italy*

Received 1986 August 1; accepted 1986 November 17

Abstract. ***N***-Body simulations have been performed to study the tidal effects of a primary stellar system on a secondary stellar system of density close to the Roche density. Two hyperbolic, one parabolic and one elliptic encounters have been simulated. The changes in energy, angular momentum, mass distribution, and shape of the secondary system have been determined in each case. The inner region containing about 40 per cent of the mass was found to be practically unchanged and the mass exterior to the tidal radius was found to escape. The intermediate region showed tidal distension. The thickness of this region decreased as we went from hyperbolic encounters to the elliptic encounter keeping the distance of closest approach constant. The numerical results for the fractional change in energy have been compared with the predictions of the available analytic formulae and the usefulness and limitations of the formulae have been discussed.

Key words: stellar systems, tidal encounters—stellar dynamics

1. Introduction

The study of encounters between galaxies has received much attention after the discovery of peculiar galaxies. Photographs of interacting galaxies by Vorontsov-Velyaminov (1959, 1977), Arp (1966) and others show that many pairs of galaxies have peculiar morphological features. Toomre & Toomre (1972) using the restricted three-body approach, showed that the tidal forces play a vital role in the dynamics of interacting galaxies and lead to the formation of such features. Ostriker, Peebles & Yahil (1974), Faber & Gallagher (1979) and Gunn (1980) have discussed dynamical evidence for the galaxies being surrounded by large haloes, often extending up to 100 kpc. This has increased our estimate for the frequency of galactic collisions and has considerably stimulated research in galaxy interactions.

* Permanent Address: Department of Mathematics, M.G.M. College, Udupi.
† Permanent Address: Centre of Advanced Study in Astronomy, Osmania University, Hyderabad 500007.

The effects of the tidal forces are not merely peripheral. The overall structure of the galaxies is also affected. The fractional increase in the total internal energy of a galaxy, $\Delta U/|U|$ provides a good measure of the change in its structure (Alladin 1965). If this is equal to or greater than unity, the galaxy would be appreciably disrupted. This ratio has been estimated by many workers using the impulsive approximation (IA) wherein the motion of the stars in the test system is neglected in comparison with the orbital motion of the systems. This approximation gives good results for energy changes even in slow hyperbolic collisions (Toomre 1977; Dekel, Lecar & Shaham 1980; Aguilar & White 1985). However, for a detailed study of the changes in the shape and mass distribution of a colliding stellar system, a self-consistent method such as the method of *N*-Body simulations is needed. This method has been extensively used to study mergers of galaxies (see Tremaine 1981, and White 1983 for reviews). Borne (1984) has determined merger times of binary galaxies using multiple three-body algorithm. In this paper we shall not consider mergers. Here we shall restrict ourselves to the cases of non-penetrating tidal encounters.

Studies of encounters between stellar systems may be divided into two categories: (a) those in which the two systems are of comparable mass, and (b) those in which there is great disparity in mass. In this paper we shall study the second category. It is convenient in this case to designate the more massive system as the primary and the less massive as the secondary (satellite). The primary has disruptive effects on the secondary while the secondary accelerates the stars in the outer parts of the primary and this leads to dynamical friction on the motion of the satellite. The former (disruptive) effect becomes more important than the latter (merging) effect as the ratio ρ/ρ_R (where ρ is the density of the satellite system and ρ_R is the Roche density) decreases (Alladin, Ramamani & Meinya Singh 1985). The case of $\rho \geqslant \rho_R$ where dynamical friction and merging are more important than disruption has been studied by Lin & Tremaine (1983) and others. In this paper we shall study the case in which the density of the satellite is close to the Roche density. We ignore the effects of dynamical friction and concentrate on how the tidal field of the primary changes the mass distribution, energy and angular momentum of the secondary. We confine ourselves to non-penetrating encounters and treat the primary as a mass point. We investigate to what extent the results of the analytic formulae derived under the assumption that the stars remain stationary (Spitzer 1958; Alladin & Narasimhan 1982; Narasimhan & Alladin 1983) agree with the numerical experiments.

In Section 2 we describe the method used and the initial conditions employed in the present simulations. The numerical results are given and discussed in Section 3. In Section 4 we give the main conclusions.

2, The Method and the Initial Conditions

2.1 *The Method*

In *N*-Body simulations we solve a system of N second-order differential equations of motion of N particles in a system simultaneously. The motions are governed by

$$\frac{\mathrm{d}^2\mathbf{r}_i}{\mathrm{d}t^2} = -G \sum_{\substack{j=1 \\ i \neq j}}^{N} \frac{m_j}{r_{ij}^3}\mathbf{r}_{ij}, \tag{1}$$

where $\mathbf{r}_{ij} = \mathbf{r}_i - \mathbf{r}_j$, m_i and $\mathbf{r}_i$ are the mass and position vector of particle i, G is the constant of gravitation. A problem arises in near collision of two particles due to the singularity when $r_{ij} \to 0$. Also on account of the restriction that N should be small to save computer time, relaxation time is reduced and the system may not mimic a real system. The relaxation time is increased by using a softened potential, given by

$$\Phi_i = -G \sum_{\substack{j=1 \\ i \neq j}}^{N} \frac{m_j}{(r_{ij}^2 + \varepsilon^2)^{1/2}} \tag{2}$$

The N-BODY 1 Code of S. J. Aarseth was used to compute the orbits of the particles interacting via this potential.

2.2 *The Initial Conditions*

We studied the disruption of the secondary stellar system (satellite system) of mass M due to the tidal effects of the primary system of mass $M_1 = 10^5 M$. The satellite system was modelled by 124 particles each of unit mass distributed randomly within a sphere of radius $R = 20$ units with the mass distribution $M(r) \propto r$. Each particle was then given a velocity equal to the circular velocity at the distance and the directions of the velocity vectors were chosen *randomly* as in ISO model of White (1978). The system so generated had zero angular momentum. Its half-mass radius R_h was nearly 10 units and with $G = 1$, V_{rms} was 2.3 units and the crossing time was about 8 units. Following White (1978) we chose $\varepsilon = 1$ in Equation (2).

The system was allowed to evolve by itself for about 7 crossing times to give a well-mixed, dynamically stable system. This system had its half-mass radius almost unchanged. The values of R_{rms} and V_{rms} were nearly 20.0 and 2.2 respectively. The radius containing 90 per cent mass was about $3R_h$. The ratio of the rms radial and tangential velocities Vr, $_{rms}/Vt$, $_{rms}$ was 0.83 indicating that the model also had elongated orbits.

In order that the density of the system may be close to the Roche density when it is at its closest approach p we chose $p = 100\ R_h$. The orbital plane was chosen as the xy-plane with the x-axis in the direction of the closest approach. Four non-penetrating encounters were simulated with encounter parameters chosen as in Table 1. V_p is the magnitude of the velocity at closest approach and e is the eccentricity of the orbit.

M_1 was placed in the orbit at a distance $r = 2p$. Beyond this distance the tidal effects are negligible. The initial relative velocity at this distance was obtained from the two-body formulae. The positions and velocities of the particles in the test system and of the point-mass perturber were computed in the centre-of-mass frame of the entire system. These were taken as the input for the N-BODY 1 Code. At various times, the essential data containing the positions and velocities of all the particles were stored for the latter processing. The computation was stopped when the system showed no further change in its properties.

3. Numerical results and discussion

The position and velocity data obtained at various times was used to study the structural changes of the system during the encounter. We found the internal energy

Table 1. Simulation parameters.

Model	e	P/R_h	V_p/V_{rms}	M/M_1
H1	3.0	100	101	10^{-5}
H2	2.4	84	101	10^{-5}
P	1.0	100	72	10^{-5}
E	0.5	100	62	10^{-5}

(binding energy), the angular momentum, the mass loss, and the change in the shape, at the end of the encounter.

Due to the strong tidal forces acting on the system during the encounter, the system loses spherical symmetry. Thus the mass distribution and shape cannot be conveniently studied with respect to the centre of mass of all the particles in the system. For this purpose we took a reference frame with its origin at the centre of mass of the most dense region defined as the region containing those particles with energy less than—rather than the average energy of—the bound particles. A particle was considered to be bound or be an escaper depending on whether

$$E_i = \frac{1}{2} m_i v_i^2 - G m_i \sum_{\substack{j=1 \\ i \neq j}}^{N} \frac{m_j}{(r_{ij}^2 + \varepsilon^2)^{1/2}} \tag{3}$$

was negative or positive. We determined the structure of the system in this frame designated as the effective frame. The mass loss was estimated from the number of escaping particles.

3.1 *Energy Increase and Mass Loss*

Fig. 1 gives the fractional energy increase $\Delta U/|U|$ and the mass loss $\Delta M/M$ as a function of time for the four models. C indicates the time of closest approach. It may be noted that the energy increase is somewhat symmetric about the closest approach. This is expected from Spitzer's (1958) theory based on impulsive approximation which leads to

$$(\Delta U)_{\text{half}} = \frac{M}{2} \int_{-\infty}^{0} (\Delta \mathbf{V})^2 \, dt = \frac{M}{2} \left(\frac{G M_1}{p^2 V_p} \right)^2 \frac{4}{3} R_{\text{rms}}^2 = \frac{1}{2} (\Delta U)_{\text{Total}}. \tag{4}$$

On the other hand, Ahmed & Alladin (1981) found that the energy transfer in a head-on collision between two identical galaxies is asymmetric with respect to the closest approach, the transfer in the second half being double that of the first half. This was because of the dynamical friction, the relative velocity of the galaxies was slower in the second half. In our case the deceleration due to dynamical friction is very small and was not considered.

In the case of parabolic and elliptic encounters we found that most of the energy increase occurred when $-\pi/2 < \theta < \pi/2$ (taking $\theta = 0$ at closest approach). This does not agree with the analytic formulae obtained under IA (Alladin & Narasimhan 1982; Narasimhan & Alladin 1983) which predict that the energy increase in this range is half the total ($-\pi < \theta < \pi$). Since $\Delta U/|U|$ predicted by these formulae for the total

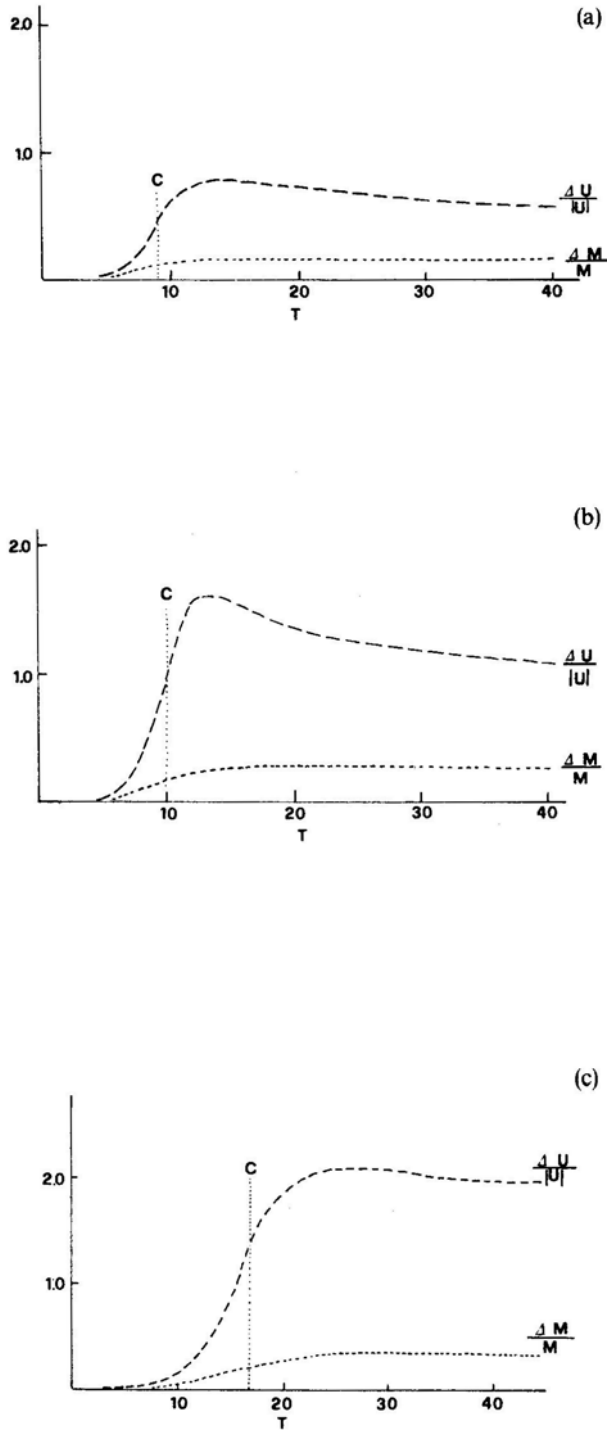

Figure 1. Fractional change in energy and fractional mass loss as a function of time for the four models (a) H1, (b) H2, (c) P, and (d) E.

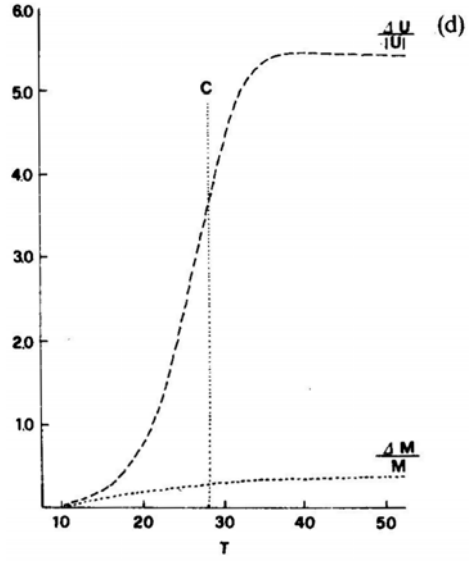

Figure 1. Continued.

encounter is reasonable, as will be discussed subsequently, it follows that IA underestimates the tidal effects near the perigalacticon and overestimates on the far side.

In Table2, we compare the values of ΔU / $|U|$ obtained in the various models with those predicted from the analytical formulae derived under IA. For fast encounters, assuming the relative orbit to be rectilinear, Dekel, Lecar & Shaham (1980) obtained from Spitzer's (1958) theory

$$\frac{\Delta U}{|U|} = \frac{8}{3}\frac{G^2 M_1^2}{p^4 V_p^2}\left(\frac{R_{\rm rms}}{V_{\rm rms}}\right)^2. \tag{5}$$

From Alladin & Narasimhan (1982) and Narasimhan & Alladin (1983), we obtain for the conic orbit

$$\frac{\Delta U}{|U|} = \frac{2\pi^2}{(1+e)^2}\frac{G^2 M_1^2}{p^4 V_p^2}\left(\frac{R_{\rm rms}}{V_{\rm rms}}\right)^2 \qquad \text{for} \quad e \leqslant 1, \tag{6}$$

$$\frac{\Delta U}{|U|} = (1+e)\langle e_i^2 \rangle \frac{G^2 M_1^2}{p^4 V_p^2}\left(\frac{R_{\rm rms}}{V_{\rm rms}}\right)^2 \quad \text{for} \quad e > 1, \tag{7}$$

Table 2. Fractional increase in the energy, fractional mass loss, and the ratio of the radii containing 90 per cent mass of the bound system to that of the whole system. $(\Delta U/|U|)_{\rm Sp}$ is obtained from Equation (5). $(\Delta U/|U|)_{\rm N+A}$ is obtained from Equations (6) or (7).

Model	$(\Delta U/\lvert U\rvert)_{N\text{-Body}}$	$(\Delta U/\lvert U\rvert)_{\rm Sp}$	$(\Delta U/\lvert U\rvert)_{\rm N+A}$	$(\lvert\Delta M\rvert/M)$	$(\Delta U_{\rm B}/\lvert U\rvert)$	$(R_{\rm B}/R)_{0.9}$
H1	0.61	0.70	0.72	0.19	0.24	0.30
H2	1.12	1.40	1.60	0.27	0.27	0.44
P	1.96	1.40	2.60	0.39	0.36	0.58
E	5.48	1.90	6.00	0.40	0.43	0.71

where

$$\langle e_i^2 \rangle = (e_1^2 + e_2^2 + e_3^2)/3,$$

$$e_1 = \frac{1}{(e+1)^{1/2}}\left[\frac{1}{(e+1)}\cos^{-1}(-e^{-1}) + \frac{2e^2-1}{e^2}\left(\frac{e-1}{e+1}\right)^{1/2}\right],$$

$$e_2 = \frac{1}{(e+1)^{1/2}}\left[\frac{1}{(e+1)}\cos^{-1}(-e^{-1}) + \frac{1}{e^2}\left(\frac{e-1}{e+1}\right)^{1/2}\right],$$

$$e_3 = \frac{2}{(e+1)^{1/2}}\left[\frac{1}{(e+1)}\cos^{-1}(-e^{-1}) + \left(\frac{e-1}{e+1}\right)^{1/2}\right]. \tag{8}$$

Equations (6) and (7) are derived on the assumption that the relative orbit is the unperturbed two-body orbit. Equation (5) is of much simpler form since the relative motion is assumed to be rectilinear with constant speed. $\Delta U/|U|$ predicted by the analytical formulae (5) and (7) agree well with the results of numerical experiments for models H1 and H2. For model P, Equation (5) underestimates $\Delta U/|U|$ while Equation (6) overestimates it. The computed value lies almost exactly in between these two estimates. For model E the numerical value is in good agreement with that predicted by Equation (6). Equation (5) underestimates it by a factor of about 3 in this case.

In Table 2 we also give $\Delta U_B/|U|$ where U_B is the binding energy of the final bound part, $\Delta M/M$, the fractional mass loss, and $(R_B/R)_{0.9}$ the ratio of the radii containing 90 per cent mass of the bound system to that of the total system. We find a linear relation of the form (Fig. 2):

$$\frac{\Delta U_B}{|U|} \simeq \frac{\Delta M}{M} \simeq 0.6\left(\frac{R_B}{R}\right)_{0.9}.$$

The first part of the result was earlier noted by Dekel, Lecar & Shaham (1980) for their A model.

The range in $\Delta U_B/|U|$ is considerably smaller than the range in $\Delta U/|U|$. This is because a large part of the transferred energy is carried away by the escaping particles, a result earlier noted by Richstone (1975). An interesting point is that as we go from the hyperbolic to the parabolic case keeping p fixed, $\Delta U/|U|$ and $\Delta M/M$ both go on increasing. But when we go from the parabolic to the elliptic case $\Delta M/M$ remains almost unchanged, but $\Delta U/|U|$ increases drastically. This is because the escaping particles in the elliptic encounter carry away much larger energy than in the case of the parabolic encounter. White (1978) found that more particles escape from parabolically colliding systems than from initially bound systems for equal mass encounters.

Aguilar & White (1985) have written a comprehensive paper on tidal interactions between spherical galaxies in which the changes in binding energy and mass are obtained both by the methods of IA and *N*-body simulations. They have considered galaxies of comparable mass and concentrated on interpenetrating collisions. They have found that Spitzer's distant-encounter formula is valid only for impact parameters exceeding 10 times the effective radius of the test galaxy. In the hyperbolic and parabolic cases that we have studied, this condition is always satisfied since the separation is much larger. Thus, Equation (5) gives good agreement with the results of numerical experiments for hyperbolic and parabolic orbits as expected.

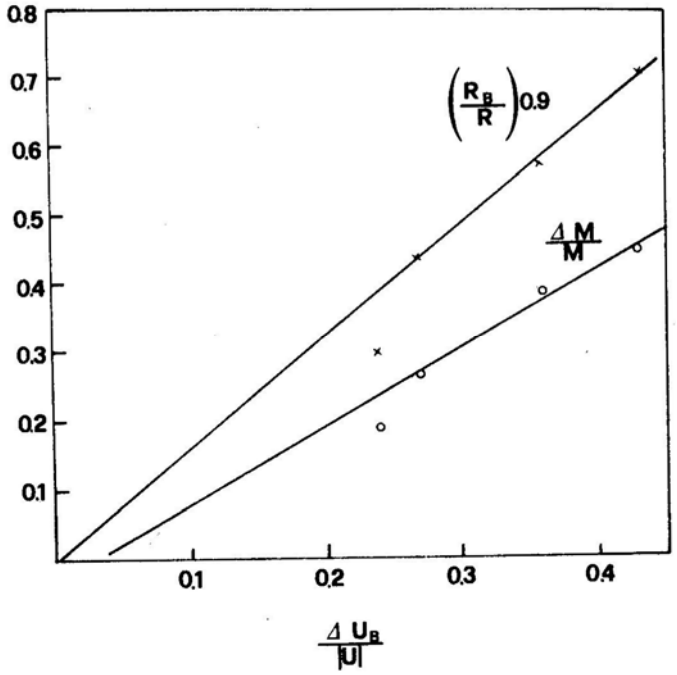

Figure 2. Relation between changes in energy, mass and size.

3.2 *Gain in the Angular Momentum*

As a result of tidal interaction, the satellite system acquires angular momentum from the orbital angular momentum of the pair. In Table 3 we give the orbital angular momentum $(L_Z)_{orb}$ of the pair, the spin angular momentum for the total system $(S_z)_{total}$ and for the bound part $(S_z)_{bound}$ after the encounter. It can be seen that only a very small fraction of the orbital angular momentum is transferred, and that most of the transferred angular momentum is carried away by the escaping particles as earlier noted by White (1979) in simulations of merging galaxies. We also note that the escapers carry away small angular momentum in large angular momentum encounters and vice-versa. Thus the angular-momentum transfer is inversely related to the orbital angular momentum.

Table 3. Angular momentum transfer from the orbital motion to the test system.

Model	$(L_z)_{orb}$	$(S_z)_{Total}$	$(S_z)_{bound}$
H1	2.8(+7)	4.0(+3)	3.6(+2)
H2	2.3(+7)	7.6(+3)	2.1(+2)
P	2.0(+7)	2.1(+4)	1.3(+2)
E	1.7(+7)	6.0(+4)	2.3(+2)

3.3 *Particle Orbits*

An idea of the change in the nature of the stellar orbits can be had from the values of $(V_r)_{rms}$ and $(V_t)_{rms}$ after the encounter. These are given for the total system and for the bound part in Table 4. Both the radial and the transverse velocities of the stars are increased as a result of the tidal interaction. Hyperbolic and parabolic encounters favour the radial motion more than the transverse motion. In bound-orbit encounters both are almost equally affected. The bound part has more transverse orbits than radial orbits even compared with the initial system. It follows that the stars in radial orbits preferentially escape.

3.4 *Radial Mass Distribution*

To study how the radial distribution of mass changes due to the encounter we find the radii containing 10 per cent, 20 per cent, *etc.* of the total mass in the effective frame. This is done for the initial system and the final system including the escapers. The results are given in Table 5. In Fig. 3 $M(r/R_h)/M$ is plotted against r/R_h where M and R_h are the initial mass and half-mass radius of the system.

We distinguish three regions in the final system: (1) the inner region containing about 40 per cent of the mass which remains practically intact; (2) the intermediate tidally distended region which extends up to the tidal radius; and (3) the region exterior to the tidal radius which is found to escape. Dekel, Lecar & Shaham (1980) also observed that the mass distribution within R_h almost remained intact and there was expansion for $r > R_h$. The figure shows that there is not much difference in the final mass distribution between models P and E.

Table 4. Radial and transverse velocities.

	Total			Bound		
Model	$(V_r)_{rms}$	$(V_t)_{rms}$	$(V_r)_{rms}/(V_t)_{rms}$	$(V_r)_{rms}$	$(V_t)_{rms}$	$(V_r)_{rms}/(V_t)_{rms}$
Initial	1.41	1.70	0.83	1.41	1.70	0.83
H1	1.82	1.81	1.00	1.05	1.84	0.57
H2	2.37	1.81	1.31	1.03	1.85	0.56
P	2.84	2.38	1.91	1.19	1.93	0.62
E	2.58	4.69	0.76	1.06	2.00	0.53

Table 5. Mass distribution before and after the encounter.

	$M(r/R_h)/M$									
Model	0.1	0.2	0.3	0.4	0.5	0.6	0.7	0.8	0.9	1.0
Initial	0.12	0.26	0.45	0.67	0.95	1.35	1.83	2.66	3.15	7.8
H1	0.18	0.30	0.46	0.70	1.06	1.59	2.64	5.91	9.4	35
H2	0.16	0.30	0.46	0.75	1.19	2.28	3.75	8.6	13.1	40
P	0.14	0.28	0.40	0.71	1.39	3.26	9.2	13.2	17.5	36
E	0.15	0.29	0.56	0.79	1.93	3.38	7.9	16.1	21.3	35

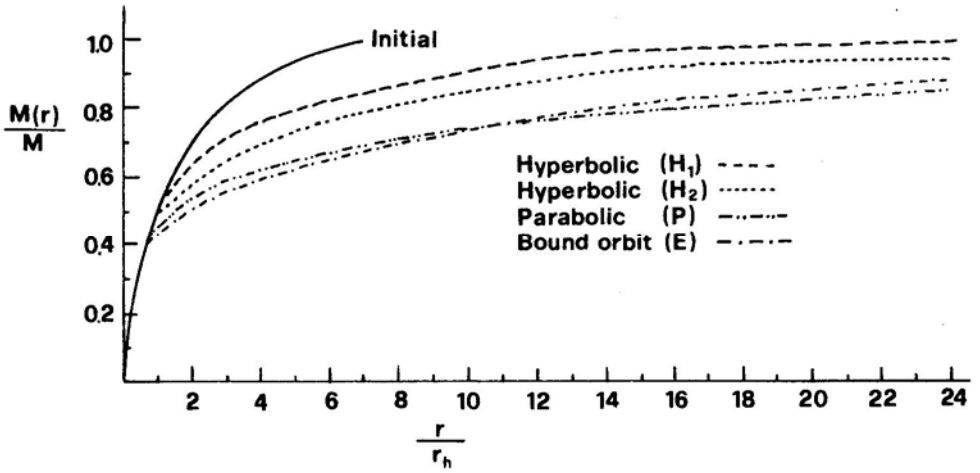

Figure 3. Mass distribution before and after the encounter for the four models.

3.5 *Tidal Radius*

The tidal radius obtained from numerical experiments is compared with those predicted from analytic formulae in Table 6. $(R_t)_{N\text{-Body}}$ is defined as the radius of the initial test system, beyond which the mass escapes in the numerical experiment. $(R_t)_{\text{King}}$ is obtained from King's (1962) formula

$$R_t = p\left(\frac{M}{M_1(3+e)}\right)^{1/3}, \tag{9}$$

and $(R_t)_{IA}$ is taken as the value of R_{rms} in Equation (6) or (7) for which $\Delta U/|U| = 1$. We note that $(R_t)_{N\text{-Body}}$ agrees well with $(R_t)_{IA}$ for hyperbolic and parabolic encounters and with $(R_t)_{King}$ for parabolic and bound-orbit encounters as expected. We also give in the table the radius of the intact sphere measured in the unit of the tidal radius. It may be noted that this fraction is smaller for the hyperbolic encounters which implies that the size of the intermediate region which produces tidal distension decreases as we go from hyperbolic encounter to elliptic encounter keeping the distance of closest approach constant. If we keep p constant, the intermediate region becomes thinner with decreasing e.

It is of interest to compare the result of the present work with that of Angeletti, Capuzzo-Dolcetta & Giannone (1983) who studied analytically the tidal linear stability

Table 6. Tidal radius and the radius of the intact sphere.

Model	$(R_t)_{N\text{-Body}}$	$(R_t)_{King}$	$(R_t)_{IA}$	R_{intact}/R_t
H1	26	15	24	0.4
H2	18	13	16	0.5
P	13	15	12.5	0.6
E	13	15	8	0.6

of a homogeneous star cluster considered as a galactic satellite. They indicated the regions of stability and instability in the v, e plane where

$$v = \frac{M_c}{M_g}\left(\frac{a}{R_c}\right)^3,$$

M_c, M_g, a, R_c, being respectively, the mass of the cluster, the mass of the Galaxy the semi-major axis of the orbit and the radius of the cluster. For a given e, three regions of v may be distinguished: (a) the region of instability when $v < v_{min}$, (b) the region of stability, where $v > v_{max}$, and (c) the transition region $v_{max} > v > v_{min}$ containing zones of both stability and instability. This work shows that in the case of the circular orbit, there is a sharp transition between regions of stability and instability and the width of the transition region increases with e.

3.6 *Change in Shape*

We can make a crude quantitative estimate for the shape of a system of particles from the values of $\langle|x|\rangle$, $\langle|y|\rangle$, $\langle|z|\rangle$. These are given for the total system and for the bound part in Table 7. We also give in the table, the expansion parameters E_x, E_y, E_z defined by

$$E_x = \frac{\langle|x_f|\rangle - \langle|x_i|\rangle}{\langle|x_i|\rangle} \quad etc.,$$

where f and i denote final and initial values. We note that the maximum expansion is always in the x direction and the least in the z direction. At the encounter we have a system flattened in the orbital plane, consistent with the gain in angular momentum in the z direction. The final bound part is, however, almost spherical in shape.

It may be noted that for the hyperbolic encounters, the expansions in the y and z directions are nearly equal. But in the case of parabolic and elliptic encounters the expansion in the z direction is considerably smaller than that in the y direction. We can summarize our results as

$$E_x \gg E_y \simeq E_z \quad \text{for} \quad e \simeq 3,$$
$$E_x > E_y \gg E_z \quad \text{for} \quad 0.5 < e \leqslant 1.0.$$

We expect E_x , E_y, E_z to be proportional to the energy increments in the x, y, z, directions. According to Spitzer's (1958) formula if $e \gg 1$ then $\Delta V_x^2 = \Delta V_z^2$ and $\Delta V_y^2 = 0$. According to Alladin & Narasimhan (1982), for $e \leqslant 1$, $\Delta V_x^2 = \Delta V_y^2 = \frac{1}{4}\Delta V_z^2$

Table 7. Expansion parameters in the three directions.

Model	Total			Total			Bound		
	$\langle\|x\|\rangle$	$\langle\|y\|\rangle$	$\langle\|z\|\rangle$	E_x	E_y	E_z	$\langle\|x\|\rangle$	$\langle\|y\|\rangle$	$\langle\|z\|\rangle$
Initial	6.6	6.6	6.6				6.6	6.6	6.6
H1	24	11	12	2.6	0.6	0.8	7.4	7.3	6.2
H2	32	15	15	3.9	1.2	1.2	6.5	5.2	5.5
P	42	26	11	5.4	3.0	0.7	4.5	3.4	4.5
E	48	32	8	6.3	3.9	0.2	4.5	4.5	4.5

A comparison of the prediction of the analytic formulae with the numerical results indicates that IA overestimates $(\Delta V_z)^2$ in every case. Since the overall estimate for ΔU predicted by IA agrees with the numerical results, it follows that IA underestimates $\Delta V_w^2 = \Delta V_x^2 + \Delta V_y^2$. The IA estimate agrees with the numerical results in predicting that $E_x \gg E_y$ for $e = 3$ but does not agree in predicting that $E_x > E_y$ for $0.5 < e \leqslant 1.0$.

IA is not satisfactory for predicting ΔV_z^2 in slow hyperbolic or bound orbit encounters. Agreement with numerical results may be achieved in a fast hyperbolic encounter. It may be noted that in IA, the term $\mathbf{V}\cdot\Delta\mathbf{V}$ is neglected and that ΔV_Z is negative for a star on the positive z-axis. The negative sign of ΔV_z acts in the direction of reducing the expansion in the z direction. That the tidal expansion in the z direction is small is consistent with Chandrasekhar's (1942) analysis for the tidal disruption of a star cluster, which shows that the disruption does not occur on account of tidal instability in the z direction.

3.7 *Escaping Particle*

In Fig. 4 we plot the number of escaping particles in each quadrant at different times. The circle on the relative orbit represents the position of the perturber. The number in each quadrant is the number of particles beyond a distance of 30 units. Almost all of them are escapers, The system first tends to get elongated towards and away from the perturber. This direction slowly rotates following the perturber's motion. A similar scenario was also observed by Miller (1984) in his study of the tidal effects on a satellite system. The satellite system was seen to get elongated towards and away from the perturber and the particles were seen to escape from the end of the bulges. Dekel, Lecar & Shaham (1980) observed that in interpenetrating encounters, the escaping particles had a preferred direction which was opposite to the direction of closest approach, whereas in distant encounters, particles escaped both towards and away from the perturber.

4. Conclusions

The main conclusions of this work are as follows:

1. The thickness of the shell between the inner intact sphere and the outer stripped region decreases as we go from a hyperbolic orbit to a bound orbit encounter, keeping the distance of closest approach fixed.
2. The estimate for $\Delta U/|U|$ obtained under IA for a conic orbit (Equations 6 and 7) is in fairly good agreement with that obtained by the numerical method for $e \geqslant 0.5$. Spitzer's formula holds for $e \geqslant 1$.
3. Although IA gives good estimates for the overall energy transfer, it does not predict correctly the components of the stellar velocity perturbations. Unless $e \gg 1$, $(\Delta V_Z)^2$ is always overestimated. In a bound orbit encounter, the error is large. The expansion parameters obtained from the numerical experiments satisfy the relations $E_x \gg E_y = E_z$ for $e \simeq 3$ and $E_x > E_y \gg E_z$ for $e \leqslant 1$. On the other hand, the IA formulae suggest $E_x = E_z \quad E_y$ for $e \quad 1$ and $E_z > E_x = E_y$ for $e \leqslant 1$.
4. In the case of bound-orbit encounter, IA underestimates the energy increase during the encounter on the perigalacticon side and overestimates on the apogalacticon side.

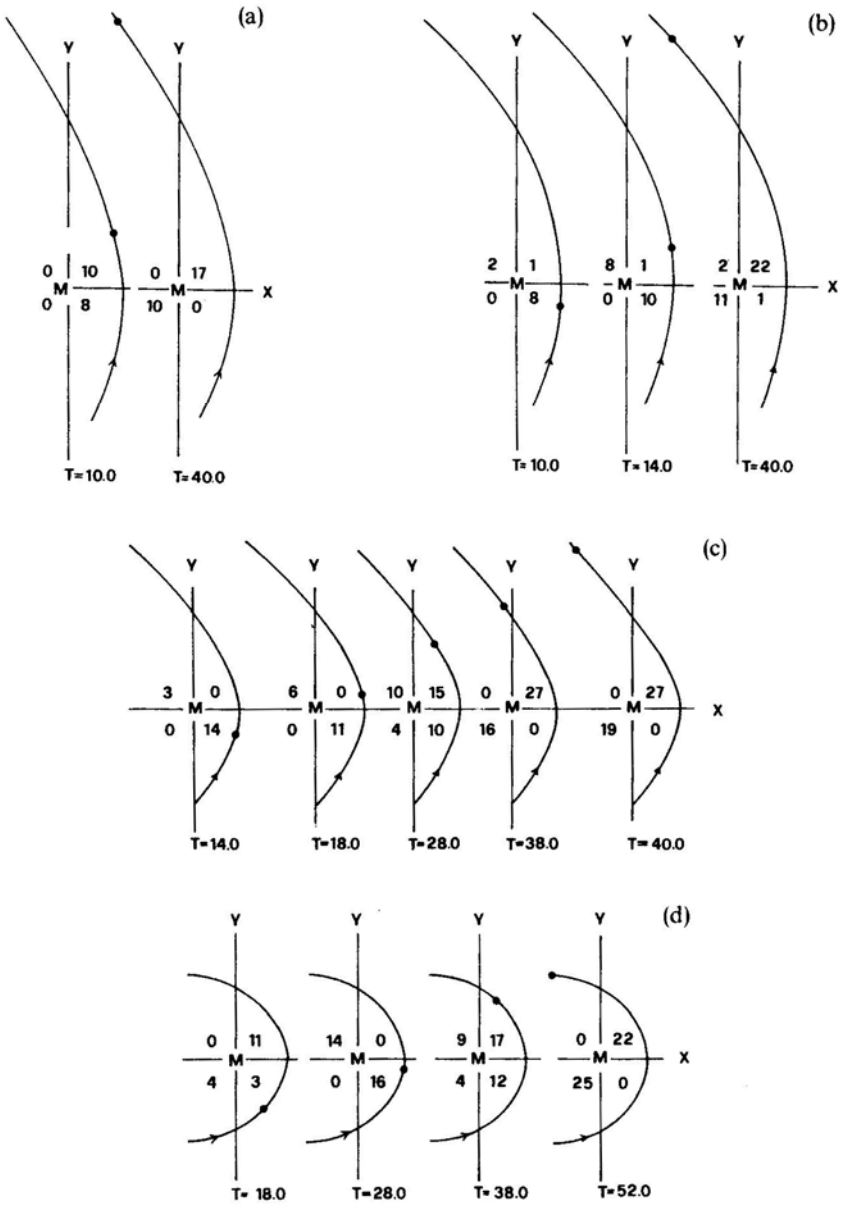

Figure 4. Number of escaping particles from various quadrants at various times for the models (a) H1, (b) H2, (c) P, and (d) E.

5 As we go from hyperbolic to parabolic encounters keeping p constant, the energy and the mass loss both increase, whereas as we go from parabolic to elliptic encounter, the energy increase continues but the mass loss remains constant.

6 An effect of the encounter is to impart spin angular momentum to the system in the same sense as that of the relative orbit. Most of this angular momentum is carried away by the escapers.

7 Tidal encounters elongate the stellar orbits in the system. Escaping stars leave the system in radial orbits. The stellar orbits in the bound part after the encounter have more circular motions than the initial system.

Many results of the present experiment are consistent with those reported by earlier workers. Detailed comparison between the results of the experiments and the predictions of the analytic formulae appears to be new.

Acknowledgments

The authors are grateful to Dr S. J. Aarseth for kindly making available the *N*-BODY 1 Code and to Dr R. K. Bhatia for useful discussions. PDR thanks the University Grants Commission, New Delhi, for providing him with a Teacher Fellowship, and to M.G.M. College, Udupi, for permitting him to make use of this opportunity. SMA is grateful to the University Grants Commission, New Delhi, for providing him with a National Fellowship. He also thanks Professor Abdus Salam, the International Atomic Energy Agency, and the UNESCO for the hospitality extended to him at the International Centre for Theoretical Physics, Trieste, where part of the work was done. He also benefitted from discussions with Professor D. W. Sciama and other scientists at the International School for Advanced Studies, Trieste.

References

Aguilar, L. A., White, S. D. M. 1985, *Astrophys. J.,* **295,** 374.
Ahmed F., Alladin, S. M. 1981, *Bull astr. Soc. India,* **9,** 40.
Alladin, S. M. 1965, *Astrophys. J.,* **141,** 768.
Alladin, S. M., Narasimhan, K. S. V. S. 1982, *Phys. Rep.,* **92,** 339.
Alladin, S. M., Ramamani, N., Meinya Singh, T. 1985, *J. Astrophys. Astr.,* **6,** 5.
Angeletti, L., Capuzzo-Dolcetta, R., Giannone, P. 1983, *Astr. Astrophys.,* **121,** 183.
Arp, H. C. 1966, *Astrophys. J. Suppl. Ser.,* **14,** 123.
Borne, K. D. 1984, *Astrophys. J.,* **287,** 503.
Chandrasekhar, S. 1942, *Principles of Stellar Dynamics,* Univ. Chicago Press.
Dekel, A., Lecar, M., Shaham, J. 1980, *Astrophys. J.,* **241,** 946.
Faber, S. M., Gallagher, J. S. 1979, *A. Rev. Astr. Astrophys.,* **17,** 135.
Gunn, J. E. 1980, *Phil. Trans. R. Soc.* **A, 296,** 313.
King, I. R. 1962, *Astr. J.*, **67,** 471.
Lin, D. N. C, Tremaine, S. 1983, *Astrophys. J.,* **264,** 364.
Miller, R. H. 1984, *ESO preprint* No. 343.
Narasimhan, K. S. V. S., Alladin, S. M. 1983, *Bull. astr. Soc. India,* **11,** 221.
Ostriker, J. P., Peebles, J. P. E., Yahil, A. 1974, *Astrophys. J.,* **193,** L11.
Richstone, D. O. 1975, *Astrophys. J.,* **200,** 535.
Spitzer, L. 1958, *Astrophys. J.*, **127,** 17.
Toomre, A., Toomre, J. 1972, *Astrophys. J.,* **178,** 623.
Toomre, A. 1977, in *The Evolution of Galaxies and Stellar Populations,* Eds B. M. Tinsley & R. B. Larson, Yale Univ. Observatory, p. 401.
Tremaine S. D. 1981, in *The Structure and Evolution of Normal Galaxies,* Eds S. M. Fall & D. Lynden-Bell, Cambridge Univ. Press, p. 67.
Vorontsov-Velyaminov, B. A. 1959, *Atlas and Catalogue of Interacting Galaxies,* Sternberg astronomical Institute, Moscow.

Vorontsov-Velyaminov, B. A. 1977, *Astr. Astrophys. Suppl.,* **28**, 1.
White, S. D. M. 1978, *Mon. Not. R. astr. Soc.,* **184**, 185.
White, S. D. M. 1979, *Mon. Not. R. astr. Soc.,* **189,** 831.
White, S. D. M. 1983, in *IAU Symp.* 100; *Internal Kinematics and Dynamics of Galaxies,* Ed. E. Athanassoula, D. Reidel, Dordrecht, p. 337.